Electrolysis induces *p*H gradients and domain orientation in agarose gels

Ariel Michelman-Ribeiro,[1,2] Ralph Nossal,[2] Ryan Morris,[1] Sarah Lange,[1] Chein-Shiu Kuo,[1] and Rama Bansil[1,*]
[1]*Department of Physics, Boston University, Boston, Massachusetts 02215, USA*
[2]*National Institute of Child Health and Human Development, National Institutes of Health, Bethesda, Maryland 20892, USA*
(Received 9 February 2005; published 26 January 2006)

We have used small-angle light-scattering (SALS), microscopy, and *p*H measurements to study structural changes produced in unbuffered agarose gels as ions migrate under applied electric fields (3–20 V/cm). Anisotropic, bowtielike, light-scattering patterns were observed, whose development occurred more quickly at higher fields. The horizontal lobes were more pronounced at higher polymer concentration. Analysis of the SALS data with a simple model of scattering from anisotropic rods in an electric field is consistent with anisotropic rodlike domains on the order of 10–15μm in length, which align perpendicular to the electric field. The anisotropic domains in the gel reach almost the same level of orientation, regardless of the field strength. Microscope imaging revealed anisotropic domains on the same length scale, also aligned perpendicular to the field. Profiles of *p*H variation across the gel, measured by video photography, indicate that the anisotropic patterns appear when the H^+ and OH^- ions, migrating in opposite directions, meet. Calculations of *p*H profiles using a model based on electrodiffusion reproduce several features of measured *p*H profiles, including the power-law dependence on the electric field of the time at which the oppositely charged fronts meet. Ions migrating from both ends of the gel produce *p*H changes that are correlated with macroscopic shrinking and orientation of the gel.

DOI: 10.1103/PhysRevE.73.011410 PACS number(s): 82.70.Gg, 82.35.Pq, 78.35.+c, 61.30.Gd

I. INTRODUCTION

Despite the wide use of agarose gels in important applications, such as macromolecular separation, little is known about how electric fields (*E*-fields) and ion migration influence the structure of these materials. In most physical explanations of electrophoresis, it is generally assumed that the structure of the agarose gel network is not perturbed in any significant way by the applied field. However, transient birefringence studies [1–3] clearly indicate that, under certain conditions, *E*-field-induced orientation effects (which depend on the magnitude of the field and duration of the pulse) occur. In low fields (2–10 V/cm), discrete regions of a gel often exhibit negative birefringence, indicating orientation of domains perpendicular to the *E*-field [1]. The orientation of domains in agarose gels may be facilitated by the existence of labile hydrogen bonds between polysaccharide fiber bundles. *E*-field effects, including deformation and collapse, also have been noted in investigations of chemically cross-linked ionic and nonionic gels [4]. It was posited in early analyses of such chemically cross-linked gels that this *E*-field-induced deformation and volume change arise due to an electrostatic pressure gradient exerted on the gel by the field [4]; later studies [5–8] indicated that the migration and redistribution of ions and resultant *p*H changes within the gel could be the cause of the collapse (or swelling). The phenomenon described in Ref. [4] potentially has many important applications (see, e.g., [9–11]).

Here we show that similar *p*H changes occur in physically cross-linked agarose gels. Additionally, we present two-dimensional small-angle light-scattering (2D SALS) data that provide evidence of domain reorganization in such materials. This phenomenon is accompanied by a macroscopic shrinking of the gel. Video microscopy of gels doped with indicator dye shows that both the domain orientation and the macroscopic volume change are linked to the migration of ions and a resultant *p*H change. Although polymer networks responding to mechanical deformation have been extensively investigated by small-angle neutron scattering, this is a report of anisotropic scattering in electrically deformed physical gels. The detected patterns are qualitatively similar to the "butterfly" patterns seen many years ago when mechanically stretched polymer films were studied by optical techniques [12], but the mechanisms by which those effects are produced are significantly different.

II. MATERIALS AND METHODS

A. Gel preparation

Powdered Seakem™ HEEO agarose (Cambrex Bio-Science, Rockland, ME) was mixed with a 6.8×10^{-3} M (0.04% w/v) NaCl solution to make 1%, 2%, and 3% w/v polymer samples. For the *p*H experiments, Hydrion™ 1–12 *p*H paper was soaked in the NaCl solution until the dye dissolved. This dye-infused solution was used to make the gel. Samples were heated in a closed container at 90 °C for 30 min and then poured into a custom-made cuvette consisting of a U-shaped Teflon™ piece separating two glass slides. The warm agarose solution was added, partially filling the cuvette. A Teflon comb was inserted to create wells at the two ends of the cuvette while the agarose solution cooled and solidified. After removing the comb, 6.8×10^{-3} M NaCl solution was added to the wells and thin platinum electrodes were placed in the wells close to the ends of the gel [see Figs. 1(a) and 2]. The dimensions of the gel were about 2 cm$\times$2 cm, with ~5 mm thickness.

*Corresponding author.

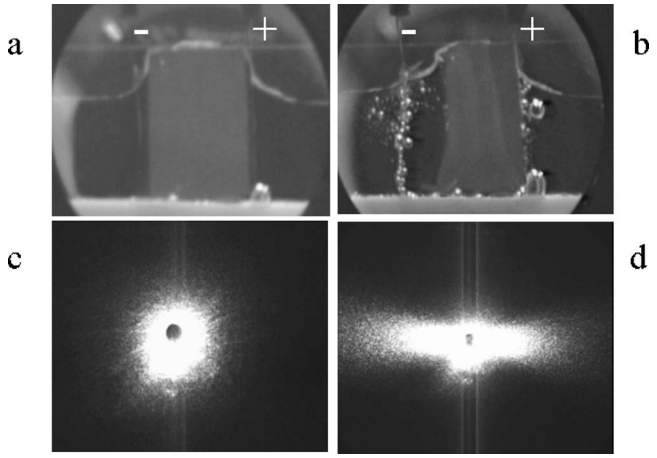

FIG. 1. Photographs of a 3% gel and the 2D light-scattering patterns produced before (a and c) and 10 min after (b and d) application of a 10 V/cm *E*-field. The vertical electrodes (+ and −), barely visible here, are more prominent in the images shown in Fig. 2. After the field is applied, gas bubbles produced by electrolysis appear and the gel shrinks away from the cathode.

B. Electrophoresis

A pulsed DC voltage ranging from 6 to 40 V was applied across the gel slab through the platinum electrodes, creating *E*-fields ranging from 3 to 20 V/cm. Unidirectional square pulses at a 1 Hz frequency from 6 to 40 V in amplitude and up to 0.9 s in duration were generated for the experiment.

Before the *E*-field was imposed, the solution and the gel contained Na^+ and Cl^- ions at a concentration of 6.8×10^{-3} M, $p\mathrm{H} \sim 6-7$. When the *E*-field was applied, the resulting electric current caused electrolysis of H_2O in the outer solution: at the cathode H_2 gas and OH^- ions were produced, whereas at the anode O_2 gas and H^+ ions appeared. The release of O_2 and H_2 from the electrodes is clearly observed as bubbles, which can be seen in the photographs in Fig. 1(b). Under the influence of the *E*-field, Cl^- and OH^- ions migrate toward the anode while Na^+ and H^+ ions migrate toward the cathode. The water level rises at the cathode because water is transported by electroendosmosis along with the H^+ ions (as H_3O^+).

C. SALS measurements

2D light scattering was recorded using a home-built SALS apparatus. A HeNe laser beam (10 mW, $\lambda = 632.8$ nm) illuminated a spot in the center of the gel and the light-scattering pattern was observed on a screen set behind the sample. This pattern was imaged by a Cohu CCD video camera and digitized by a frame grabber (Matrox Intellicam) for analysis. For each sample, we followed the time evolution of the pattern by analyzing video frames over a total run of about an hour. The direction of propagation of the incident beam (**x**), the vertical polarization vector (**z**), and the *E*-field (**y**) define a set of orthogonal axes. The scattered intensity for a given scattering vector **q** (magnitude $q = (4\pi n/\lambda)\sin(\theta/2)$, with n being the refractive index, λ the wavelength of the incident light, and θ the scattering angle) was measured in the y-z plane (the plane of the screen). The measured intensity was represented in polar coordinates as $I(q,\Omega)$, with Ω denoting the azimuthal angle measured in the y-z plane relative to the y axis (the direction of the *E*-field). To measure the change in scattering due to the applied *E*-field, the excess scattered intensity $\Delta I(q,\Omega) = I(q,\Omega) - I_{\mathrm{bkgr}}(q,\Omega)$ was calculated by subtracting I_{bkgr}, the intensity with no applied field.

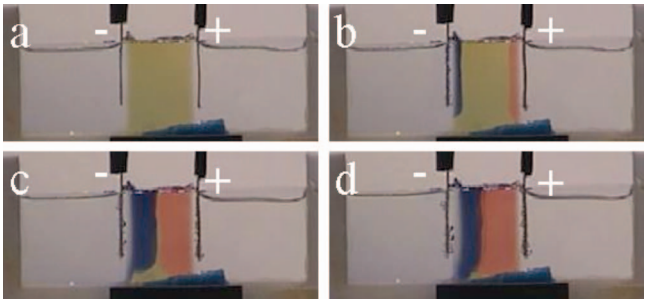

FIG. 2. (Color) Photographs of the gel before the *E*-field (10 V/cm) is applied (a), and as acidic (pink) and basic (blue) fronts move across the gel at (b) 27 s, (c) 81 s, and (d) 118 s after the field is applied. The yellowish color indicates neutral *p*H.

D. *p*H profile measurements

A second video camera, mounted in front of the sample cell, was used to photograph the entire sample in color and visually record *p*H fronts. The positions of the gel boundaries, as well as the red and blue (acidic and basic) fronts, were determined from the recordings. Changes in gel structure observed by video photography and by light scattering were unaffected by the presence of dye. We simultaneously followed the evolution of the *p*H and the light-scattering changes while ions migrated due to the pulsed *E*-field.

III. RESULTS AND ANALYSIS

Figure 1 shows a 3% gel before and after application of the *E*-field and the corresponding light-scattering patterns produced. Before the field is applied, the gel is optically uniform [Fig. 1(a)] and the light-scattering pattern is isotropic [Fig. 1(c)]. A few minutes after the field is turned on, a highly anisotropic pattern forms, as shown in Fig. 1(d). Video photographs of the gel [e.g., Fig. 1(b)] show a turbid region arising near the center of the gel at approximately the same time as the anisotropic pattern of light scattered from that region appears. The two-lobed light-scattering pattern continues to grow in intensity and visibly extends to higher scattering angles for several minutes, after which the pattern starts to shrink. The gel reveals an intense speckling, which suggests that the polymer chains move locally as fluid flows through the sample.

Photographs of the *p*H fronts are shown in Fig. 2. Before the field is applied, the gel is a yellowish color, indicating a *p*H close to neutral [Fig. 2(a)]. Once the field is turned on, the dye changes color to pink and blue near the electrodes, indicating acidic ($p\mathrm{H} \sim 3$) and basic ($p\mathrm{H} \sim 11$) conditions, respectively [Fig. 2(b)]. After a time delay that depends on

the magnitude of the *E*-field, these fronts meet and form a neutral zone [Fig. 2(c)]. It is in this region that the *p*H gradient is maximal. After the two ion fronts meet, a macroscopic shrinking begins at the cathode end. The positions of the shrunken edge, relative to its original position, were determined from photographs of the gel. At the anode end, there is no observable movement of the gel edge. We have tried a limited range of ionic strength variation (0.02–0.2% NaCl), and have found that the lower the salt concentration, the weaker the intensity of the scattering pattern and the shorter the pattern lasts. If the gel contains salt while the external solution does not, the SALS pattern is very dim and no neutral *p*H zone can be discerned. Moreover, if neither the gel nor the external solution contains added salt, there is no effect whatsoever. When a buffer is employed instead of a salt solution, the anisotropic scattering pattern appears, but only after a significant delay, which, we believe, is due to the destruction of the buffer by the ions that are produced during electrolysis (data not shown).

None of the effects described in this paper appeared when we reduced the potential difference to below the ionization potential of water, keeping the *E*-field constant by decreasing the distance between the electrodes. Thus, the effects are related to electrophoretic migration of the OH^- and H^+ ions produced during the electrolysis of H_2O, and not to *E*-field-induced changes in the gel. However, the *E*-field is important in that it facilitates the creation of a high-*p*H gradient near the center of the gel. If acidic and basic solutions are allowed to simply diffuse into the gel from opposite sides over a period of a few hours, no structural changes in the gel are observed. This is not surprising, as diffusion in the absence of an *E*-field is very slow, as has been reported in Ref. [3]. Similarly, gels immersed in either 0.1 M HCl or 0.1 M NaOH did not swell or shrink over a period several days. Interestingly, in the electrophoresis experiments it is important to keep the level of the solution below the top of the gel; if the solution level is higher, the ions bypass the gel and none of the described effects occur. This confirms that the observations reported here are caused by ions migrating within the gel, and that other factors, such as O_2 and H_2 gas bubbles produced by electrolysis and the hydrostatic pressure differences due to electroendosmosis, are of negligible importance. Note that our system differs markedly from those conventionally employed for DNA electrophoresis, in that our gel is not entirely submersed and our solutions are not buffered.

To quantify the effects of ion migration, we measured the distance across the gel that the acidic and basic *p*H fronts travel during the experiment. In Fig. 3, we see that these fronts meet near the center of the gel. From the distance that the fronts travel, we were able to calculate their velocities. Repeating this experiment, we determined the velocity of the fronts as a function of *E*-field. This follows a linear relationship, and allows us to extrapolate a threshold value, E_0, that needs to be exceeded before the fronts form and move (Fig. 4). Although there is some uncertainty in this value, we find $E_0 \sim 1.88$ V/cm. In Fig. 5, we plot the times at which the *p*H fronts meet and the times at which the anisotropic light-scattering patterns first appear, as a function of field, adjusted for E_0. The slope of the linear fit (on a log-log plot) to the *p*H

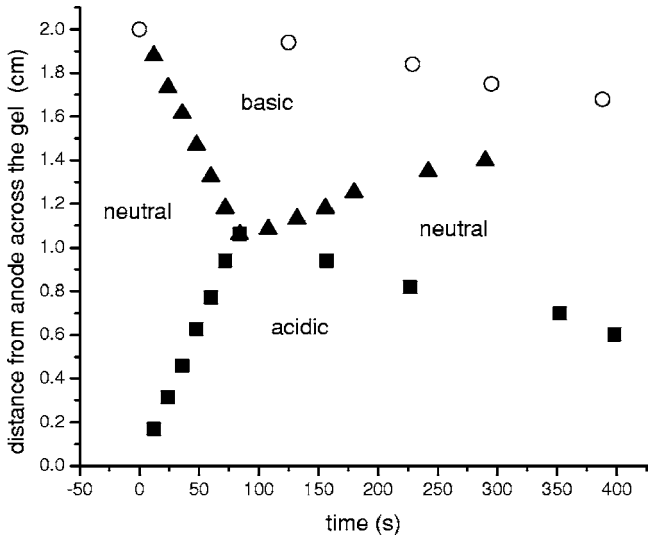

FIG. 3. Plot of acidic (squares, *p*H=3) and basic (triangles, *p*H=11) fronts across the gel as a function of time after the field (E=10 V/cm) is applied. Initially, most of the gel has a neutral *p*H. When the fronts meet, a neutral zone is formed, which widens over time as the leading edges of the acidic and basic regions recede. The edge of the gel (open circles) shrinks from the cathode as the fronts migrate (volume change ~15%).

data is −0.92, whereas that of the SALS data is −0.89. The agreement between these values, which are determined by two independent methods, suggests that these techniques are measuring related phenomena. Additionally, as shown in Fig. 3, the gel matrix located in the basic region can be seen to shrink from the cathode, thus providing visual evidence that the *p*H changes and light-scattering observations are correlated with macroscopic contraction of the sample.

A. Calculation of *p*H profiles

What is the origin of the deformation of the gel? Chemically cross-linked polyelectrolyte gels have been extensively

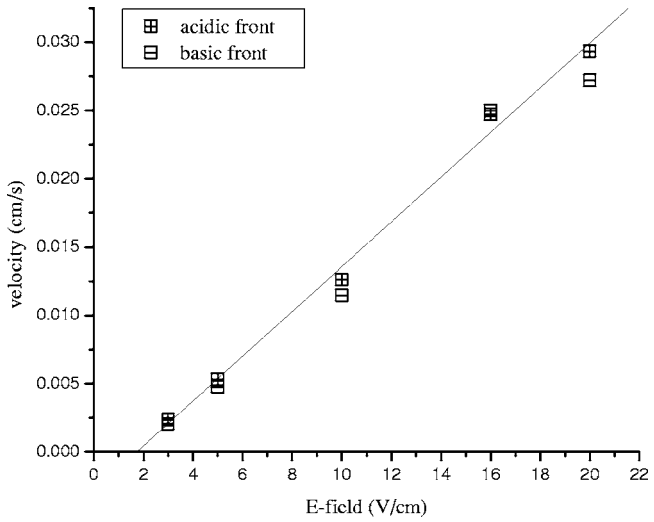

FIG. 4. Velocity of the acidic and basic fronts as a function of the applied *E*-field. The straight line is a linear fit to the acidic front.

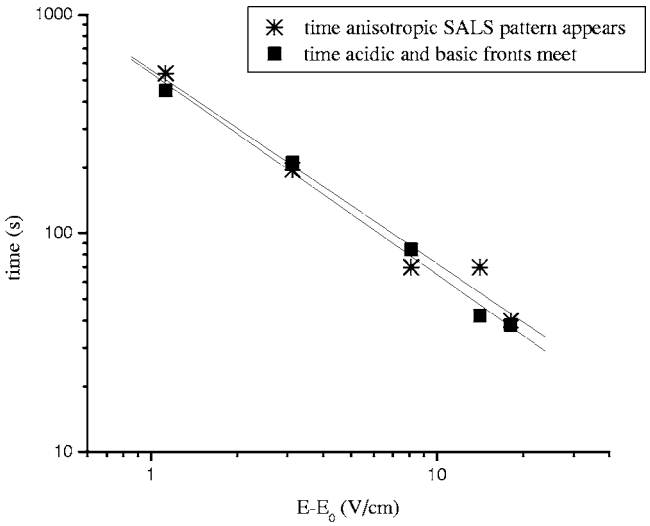

FIG. 5. Times when the acidic and basic fronts meet and the anisotropic SALS pattern appears, shown as a function of the applied *E*-field minus the threshold *E*-field required to move the ions toward the oppositely charged electrode.

studied in terms of their electromechanical responses in electric fields [6,7,13]. Agarose, however, is a physical gel, with fiber bundles held together through hydrogen bonds, which can be more easily rearranged in an *E*-field. HEEO agarose, which is used in these studies, contains somewhat more than 0.14% ester sulfate groups attached to the chain backbone [14] which, along with other backbone "impurities" and dissociable sugar hydroxyls (at high *p*H), may cause it to behave as a weak polyelectrolyte. When gels are subjected to external *E*-fields, positively charged, dissociated ions migrate toward the cathode, dragging associated water molecules with them. Grimshaw *et al.* [6] developed a model that accounts for ionic transport within a polyelectrolyte gel membrane in terms of electrodiffusion phenomena, dissociation of membrane charge groups, intramembrane fluid flow, and mechanical deformation of the gel network. The coupling of chemistry with ion flow complicates matters. For example, if the local *p*H is greater than the *p*K of atomic groups that can release H^+ ions, the resulting charges on the agarose strands will interact with, and slow, the movement of the ions in solution; moreover, the redistributions of ions can result in expansion or contraction of the gel [6]. Hirose *et al.* [7] developed a similar model, applicable for studying ionic and nonionic gels of arbitrary thickness. They, too, concluded that ion migration causes *p*H differences along the gel and asserted that electro-osmotic effects cause gel shrinking.

As Hirose *et al.* [7] show, the analysis of this system includes numerous equations that, in general, are coupled to each other through requirements of electroneutrality, *p*H-dependent dissociations of ions from the gel lattice, and the dissociation equilibrium of water and solutes. In general, these equations need to be solved numerically, but the calculations can be extremely complicated and the physics underlying the results may be difficult to discern. The simplest situation is that of a nonionic gel in an electrolyte solution of nonreactive ions. The model of Hirose *et al.* [7] (see the Appendix) indicates that the concentration, $C_M(x,t)$, of a positive ionic species M is given as a function of position x in the gel, at time t after the E-field is applied, by

$$C_M(x,t) = A_0 e^{2px} + e^{px-rt}\left\{\sum_{n=1}^{n=\infty} B_n\left[\frac{k_n}{p}\cos(k_n x) + \sin(k_n x)\right]e^{-D_M k_n^2 t}\right\}, \quad (1)$$

where A_0, B_n, k_n, D_M, p, and r are

$$A_0 = \frac{c_M^0 2pL}{e^{2pL}-1}, \quad B_n = \frac{c_M^0 4k_n[1-(-1)^n e^{-pL}]}{Lp^2\left(1+\frac{k_n^2}{p^2}\right)^2},$$

$$k_n = \frac{n\pi}{L}, \quad D_M = \frac{\mu_M RT}{z_M F}, \quad p = \frac{\nu_M}{2D_M}, \quad r = \frac{\nu_M^2}{4D_M}.$$

Here L is the length of the gel, μ_M is the mobility of the ion, $\nu_M = \mu_M E$, and C_M^0 is the (uniform) concentration of the ion M before the field is impressed across the sample. The concentration of the negative ion is calculated in the same way after substituting L-x for x in Eq. (1). By applying the conditions of electroneutrality and dissociation equilibrium of water, we obtain the concentration of H^+ ions, C_{H^+}, and thus the *p*H (see the Appendix). A more complicated calculation for ionic gels, which yields similar results, has been reported in Ref. [7]. Since agarose has only a small amount of charged groups, we used the equations given above for a nonionic gel to compute the *p*H profiles, for several values of *E*. The parameters were the initial concentrations of Na^+ and Cl^- ions and their mobilities (which we approximate as if in water). After calculating $C_{Na}(x,t)$ and $C_{Cl}(x,t)$ according to Eq. (1), we applied the electroneutrality equation locally to get the concentration of H+ ions, and thus the *p*H, as a function of time and position in the gel.

In Fig. 6(a), we show typical results of calculations of the locations of the *p*H 3 and *p*H 11 fronts within the gel as a function of time. The movements of the fronts are qualitatively similar to those observed in the experiments (see Fig. 3). We also determined the times at which these acidic and basic fronts meet, for several values of *E*-fields, as shown in Fig. 6(b). Results of calculations [Fig. 6(b)] show the same linear trend as the data (Fig. 5), as indicated by a slope close to −1 on log-log plots. Moreover, the absolute values of the calculated times and those derived from the data agree to within a factor of ~2–3. This difference, between experiment and calculations, is not surprising given that the model neglects the production of H^+ and OH^- at the electrodes. In addition, the *E*-field and the ionic mobilities in the gel are likely to be different from the external field and free-solution mobilities.

B. Anisotropic 2D small-angle light-scattering patterns

To investigate the structural changes that occur in the gel during electrophoresis, we turn to the SALS data. As discussed earlier [see Figs. 1(c) and 1(d)] some time after the *E*-field is applied the isotropic light-scattering pattern

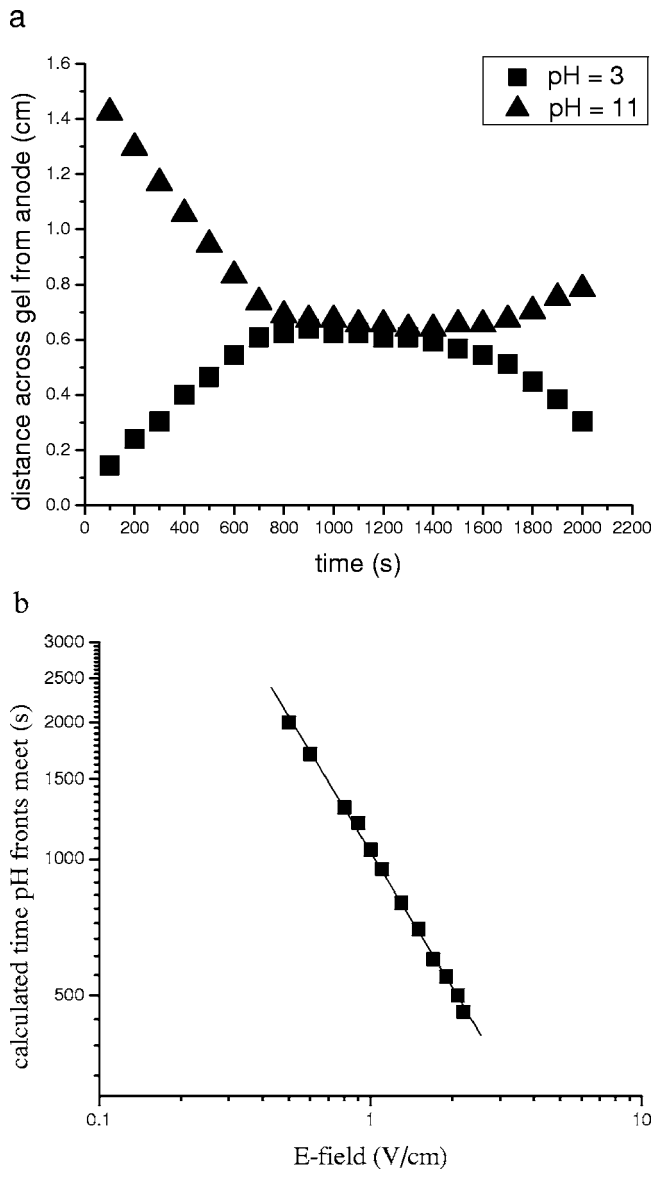

FIG. 6. (a) Positions of the fronts of constant *p*H (squares, *p*H =3; triangles, *p*H=11) within the gel as a function of time, calculated with $E=1.1$ V/cm, $C_{Na}^{0}=C_{Cl}^{0}=6.8\times10^{-3}$ M, and the free solution values $\mu_{Na}=5.2\times10^{-4}$ cm^2/V, $\mu_{Cl}=7.9\times10^{-4}$ cm^2/V. (b) Times at which the *p*H=3 and *p*H=11 fronts meet, as a function of *E*-field, according to calculations with Eq. (1). The slope of the fit to the data is −0.99 on the log-log plot.

changes and starts to display horizontal lobes. In order to better illustrate the effects of the applied field, we show, in Fig. 7, a typical excess light-scattering pattern obtained after the bowtie pattern has developed. The figure also shows the light-scattering geometry. To quantify the 2D light-scattering pattern, we use two 1D plots: the q dependence of the excess scattered intensity $\Delta I(q,\Omega)=I(q,\Omega)-I_{bkgr}$ along the radial line $\Omega=0$, and the azimuthal plot, which gives the variation of the intensity along a ring at fixed q (Fig. 7 shows $q=1.8$ μm^{-1}). Examples of such plots (at $t=160$ s) are shown at the bottom of Fig. 7. The horizontal lobes can be characterized by the intensity, $\Delta I(q,\Omega=0)$, and the full width at half height, $\Delta\Omega$ of the peak in the azimuthal plot at a fixed value of q.

As mentioned earlier, the bowtie pattern gets more intense and broadens slightly with increasing time, reaching a maximum at t^*, after which it begins to decay. To illustrate these observations we show [in Fig. 8(a)] the q dependence of the excess scattered intensity along the axis of the horizontal lobe (i.e., $\Omega=0$). The figure shows that the intensity increases at all values of q during this period. The increase in $\Delta I(q,\Omega=0)$ at a fixed value of $q=1.8$ μm^{-1} is shown in Fig. 8(b). The latter figure also shows that the width of the horizontal lobes, $\Delta\Omega$ (represented by horizontal bars) increases slightly with time.

Increasing the *E*-field causes the pattern to appear earlier. This is not surprising, since the velocity of ion migration is proportional to the field. The effects of varying the *E*-field on the SALS patterns are summarized in Fig. 9, where we see that the time evolution of $\Delta I(q,\Omega=0)$ is virtually the same for the different values of E. In fact, the curves in Fig. 9(a) can be superposed by simply shifting along the time axis. Since the intensity saturates to approximately the same final value, irrespective of E, the gel domains must reach the same maximum orientation. This is further confirmed in Fig. 9(b), which shows approximately *E*-field-independent azimuthal distributions of the excess scattered intensity, $\Delta I(q,\Omega)$, obtained at times t^* when the horizontal lobes had reached their maximal saturation value.

Qualitatively similar observations were obtained when we varied the gel concentration and pulse duration. The horizontal lobes were more pronounced at higher gel concentrations (2% and 3%), while both vertical and horizontal lobes were seen in 1% gels. Our observation of anisotropic light-scattering patterns from oriented gel domains also agrees with the strong birefringence seen in the measurements of Stellwagen and Stellwagen [2], who interpreted their results in terms of slow rotational reorientation of gel structures in low *E*-fields. The compression of the gel along the direction of the *E*-field due to forces exerted on the sulfate and other negative charges fixed on the agarose fibers, and the transport of water in the direction of the cathode, might also contribute to the alignment of the gel domains perpendicular to the *E*-field direction.

C. Model calculation of 2D SALS patterns

Anisotropic light-scattering patterns are indicative of scattering from elongated structures. Since, in our case, the scattering is greater in the horizontal direction, the scatterers are preferentially oriented vertically, i.e., at right angles to the applied field. Agarose gels are made up of bundles of polysaccharide fibers (held together by labile hydrogen bonds) [15,16], which have been treated as rods in simplest approximations [17–20]. To analyze the field-induced 2D scattering patterns, we consider, as an illustrative model, scattering from electrically anisotropic, infinitesimally thin rods of length L, with the probability of orientation about an angle Θ given by a Boltzmann distribution. Rigid-rod models have been used before to describe both birefringence data [2] and depolarized light scattering from optically aniso-

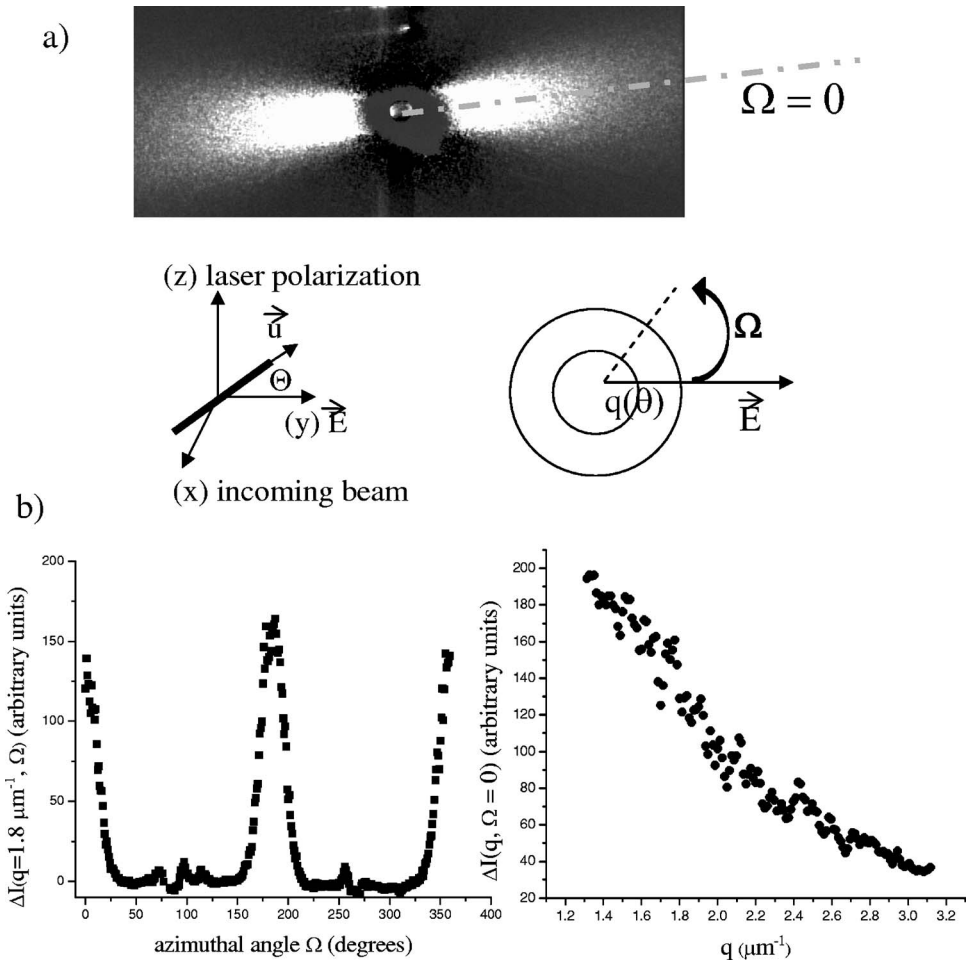

FIG. 7. The 2D scattering imaged in the y-z plane, and its representation in terms of the scattering angle θ, and the azimuthal angle Ω. (a) The 2D SALS pattern of the excess scattered intensity $\Delta I(q,\Omega)$, along with diagrams defining the orientation of a rod with respect to the lab frame (left) and the 2D scattering geometry (right). The direction of the incoming beam, the E-field, and the polarization of the incident beam define the lab frame (x,y,z). For comparison to a theoretical model of scattering from rods (discussed later in the text), we show a rod whose long axis (pointing in the direction $\mathbf{u}$) forms an angle Θ with the y axis. To clarify these angles, we show a set of circles drawn in the y-z plane, where each circle corresponds to a fixed value of θ (or equivalently, q). The azimuthal angle Ω is measured relative to the direction of the E-field, which is indicated by a dashed line in the image of the scattering pattern. (b) The azimuthal plot of $\Delta I(q=1.8\ \mu\mathrm{m}^{-1},\Omega)$ vs Ω at fixed $\mathbf{q}$ (left) and the q-dependence of $\Delta I(q,\Omega=0)$ measured along the long axis of the bowtie pattern (right).

tropic polymer films [12]. As a first approximation, the anisotropic contribution to the scattered intensity may be written as

$$I(q,\Omega) \equiv I(\theta,\Omega) = NS(q)P(\theta,\Omega), \tag{2}$$

where θ is the angle between the incident and scattered beams in the x-y plane, Ω is the azimuthal angle in the y-z plane with respect to the y axis, and N is a constant (see Fig. 7 for a sketch of the geometry). We employ, as the structure factor,

$$S(q) = S_0/(1 + q^2\xi^2 + \kappa q^4), \tag{3}$$

which other investigators have used to describe the interaction of a semidilute solution of rigid rods whose interactions are characterized by a correlation length ξ [21]. All azimuthal anisotropy is accounted for via the intraparticle form factor, $P(\theta,\Omega)$.

The form factor for rods having a Boltzmann distribution of the orientation angle Θ can be written as [22]

$$P(\theta,\Omega) = \frac{1}{2\pi\int_0^{\pi} d\Theta \sin\Theta e^{\gamma\cos^2\Theta}} \int_0^{2\pi} d\phi \int_0^{\pi} d\Theta \times \sin\Theta e^{\gamma\cos^2\Theta}\left[j_0\left(\frac{kL}{2}\mathbf{q}\cdot\mathbf{u}\right)\right]^2, \tag{4}$$

where $j_0(x)=x^{-1}\sin(x)$. The term within the square brackets is the form factor for a single rod oriented at an angle Θ relative to the y axis with $k=(2\pi n)/\lambda$, where λ is the wavelength of the incident light, and n is the refractive index of the medium (assumed here to be that of the solution in which the gel is formed). The vectors $\mathbf{q}$ and $\mathbf{u}$ are the scattering vector and unit vector along the rod axis, respectively (see Fig. 7). Their dot product can be written as

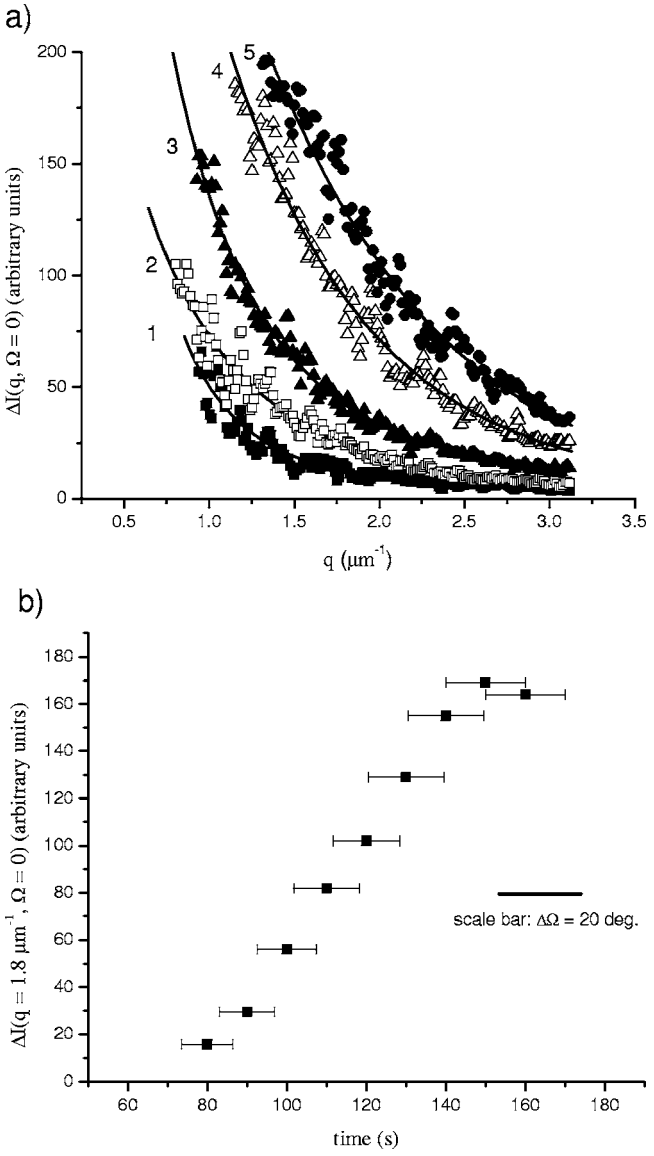

FIG. 8. (a) The q dependence of $\Delta I(q,\Omega)$ along $\Omega=0$ for a 3% gel, shown for various times after an E-field of 10 V/cm is applied (see Table I). The solid lines are calculated as described later in the text. Note that curve 5 is the same as that shown in Fig. 7(b). (b) Peak value (solid square) and peak width at half-maximum (horizontal bar) of the azimuthal intensity at $q=1.8\ \mu\mathrm{m}^{-1}$ ($\theta=8°$), as a function of time after an E-field of 10 V/cm is applied. (Note the scale for $\Delta\Omega$.)

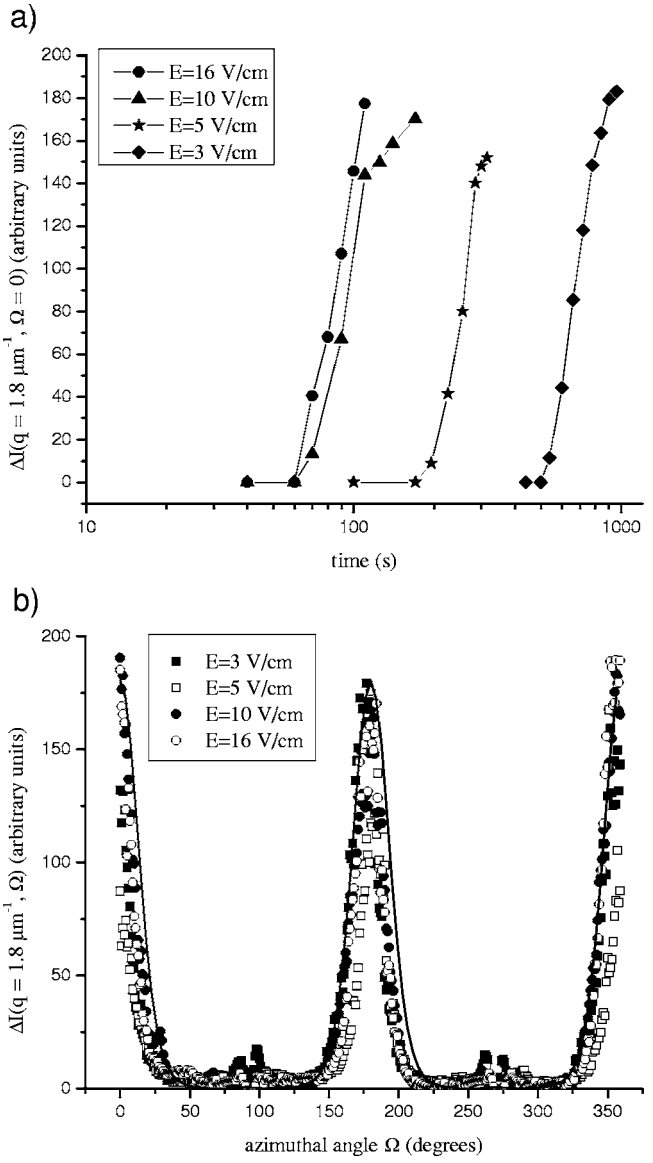

FIG. 9. (a) Maximal values of azimuthal intensity, $\Delta I(q,\Omega=0)$, for $q=1.8\ \mu\mathrm{m}^{-1}$ ($\theta=8°$), plotted as a function of time for several values of applied E-field (agarose concentration, 3% w/v). (b) Entire azimuthal plot of the scattered intensity, for the same values of E-field. All data shown here were taken at time t^* when the lobes had grown to their maximum intensity. [Solid line calculated from Eqs. (4)–(6) with $L=15$, $\gamma=-12$, as discussed later in the text.]

$$\vec{\mathbf{q}}\cdot\vec{\mathbf{u}} = (1-\cos\theta)\sin\Theta\sin\phi - \sin\theta\cos\Omega\cos\Theta - \sin\theta\sin\Theta\sin\Omega\cos\phi, \tag{5}$$

where θ is the scattering angle and ϕ is the angle the rods make with the y-z plane. When $\phi=0$, the rods lie parallel to the y-z plane, and $\mathbf{q}\cdot\mathbf{u}=-\sin(\theta)\cos(\Omega-\Theta)$. γ is an orientational order parameter for the rods, and $\gamma=0$ corresponds to rods oriented randomly at all angles. For negative γ, the dependence of $P(\theta,\Omega)$ on Ω for fixed θ (i.e., fixed q) reveals horizontal lobes, as seen in our data (Fig. 7). We evaluated the three-dimensional (3D) form factor [Eq. (4)] and also the 2D version, for rods oriented such that $\phi=0$. The 2D equation gives a better fit to our data, so we present here the analysis for coplanar rods.

As previously mentioned, Fig. 8(a) shows the q dependence, for $\Omega=0$, of the excess scattered intensity $\Delta I(q,\Omega)=I(q,\Omega)-I_{\mathrm{bkgr}}$ at various times t, after an E-field of 10 V/cm is applied (I_{bkgr} here is taken to be the isotropic contribution to the scattered intensity, obtained from the gel with no applied field.). We compared the measured excess scattering to calculated values of the anisotropic contribution, using Eqs. (2)–(5) for coplanar rods [$\phi=0$ in Eq. (5)] with appropriately chosen parameters. The length of the rod was determined by fitting the isotropic scattering $I_{\mathrm{bkgr}}(q)$ in

TABLE I. Time dependence of orientational order.

Curve No. [see Fig. 8(a)]	Time after E-field applied, t (s)	γ
1	80	−0.5
2	100	−1.5
3	120	−4
4	140	−8
5	160	−12

the absence of the E-field using Eqs. (2)–(4) with $\gamma=0$. We found $L=15$ μm. To calculate the excess scattered intensity $\Delta I(q,\Omega)=I(q,\Omega)-I_{\mathrm{bkgr}}$ at various times, we kept L fixed and varied γ. For each t, an appropriate value of γ was determined by matching the peak values of $\Delta I(q,\Omega)$, for $q=1.8$ $\mu\mathrm{m}^{-1}$, to the data (see Table I). Since the parameters NS_0, ξ, and κ [which appear in Eqs. (2) and (3)] may also depend on time, these were determined by fitting $S(q)$ to $\Delta I(q,\Omega)/P(\theta,\Omega)$, with the form factor $P(\theta,\Omega)$ calculated from Eq. (4). The calculations of $\Delta I(q,\Omega=0)$ at various times are shown, along with the data, in Fig. 8(a). The values determined for NS_0, ξ, and κ (which show no clear pattern) are of the order of 10^2, 1 μm, and 0.02 $\mu\mathrm{m}^4$, respectively. However, the parameter $|\gamma|$ is seen to increase quadratically with time (see Table I). Correspondingly, the average orientational order parameter, $\phi(\gamma)$, defined as [22]

$$\Phi(\gamma)=2\pi\int_0^{\pi} f(\Theta,\gamma)\left[\frac{3\cos^2\Theta-1}{2}\right]\sin\Theta d\Theta, \qquad (6)$$

where $f(\Theta,\gamma)$ represents the distribution of rod angles, changes from 0 (unoriented rods at $t=0$) to −0.45 at $t=160$ s (the value is −0.5 when all rods are aligned perpendicular to the E-field).

The expression for $P(\theta,\Omega)$ for coplanar rods, given by Eq. (5) with $\phi=0$, has a simple form when γ is a large negative value. In such case, the only values of Θ for which there are significant contributions to the integrals are those close to $\Theta=\pi/2$, where $\cos\Theta\approx 0$. For those values, $\mathbf{q}\cdot\mathbf{u}\approx-\sin\theta\cos\Omega$, independent of Θ so $P(\theta,\Omega)$ can be approximated as

$$P(\theta,\Omega)\approx|j_0[(kL/2)\sin\theta\sin\Omega]|^2, \qquad (7)$$

which has maxima at $\Omega=0°$ $\Omega=180°$, and $\Omega=360°$, as observed in our data. The half maximum of $P(\theta,\Omega)$, as given by Eq. (7), occurs when $j_0=0.707$, i.e., when $|(kL/2)\sin\theta\sin\Omega|\approx 1.4$. Data in Fig. 9(b) indicate a half maximum occurring when $\Delta\Omega$ ranges between 11.7° and 8.1°, from which we determine $L\approx 7-11$ μm, similar to values obtained by fitting the scattering from gels in the absence of E-fields, and also close to the values inferred from microscopy data discussed later (see Fig. 10).

We emphasize that our model for the additional scattering due to the anisotropic gel structure is but a first approximation. Clearly the anisotropic domains in the gel are not infinitesimally thin nor are they of uniform length. The gel likely contains flexible, oblong domains of finite widths and various lengths. Moreover, the structure factor given by Eq. (3) pertains to a semidilute solution (which is not the case here) and ignores the orientation of the rods (domains) with respect to each other. It is possible that the domains are changing in size as the gel compresses. The effects of interparticle scattering may need to be included, as has been investigated in a recent publication that deals with determining nematic order in assemblies of thick, hard rods [23]. The model also leaves out additional contributions to scattered light intensity from thermal fluctuations and heterogeneities in the structure of the gel. Nonetheless, this simple model is able to reproduce the dominant feature of the light-scattering patterns, namely, high azimuthal intensity in the horizontal direction [see Fig. 9(b)], and serves to support our inference that the domains are rodlike and that they orient perpendicular to the field.

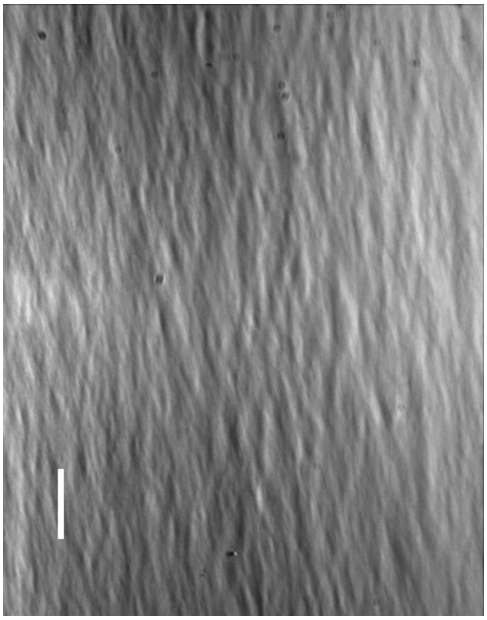

FIG. 10. Microscope image of the "neutral zone" seen in a 2% gel when subjected to a 10 V/cm electric field. Vertically aligned domains (aligned perpendicular to the applied field) can be seen (scale bar: 10 μm).

D. Microscopic observation of domains

Oriented domains can also be discerned when using an inverted optical microscope to examine the gels in an E-field. We used a custom-designed microscope chamber with electrodes immersed in the salt solution next to the gel slab. The chamber design was similar to that employed in the SALS study, except that one broad surface of the gel was free, whereas in the SALS study both broad surfaces were contiguous with glass slides. Large anisotropic domains were observed in the neutral zone near the center of the sample (Fig. 10). These anisotropic regions were very uniformly oriented perpendicular to the applied field direction. Domains in the 2% gel, which are similarly observed in 1% and 3% gels, are on the order of 10 μm in length and about 2–3 μm in thickness. These are comparable to the length scales obtained

in our earlier analyses of SALS data ($L=15$ μm and correlation length$=1$ μm). This domain length is also similar to that reported from transient electric birefringence measurements [1–3].

IV. SUMMARY AND DISCUSSION

We have found that when an electric field is imposed across unbuffered agarose gels prepared in salt solution of low ionic strength, large *p*H gradients soon arise within the samples. Light scattering from such gels is characterized by the appearance of "butterfly" or "bowtielike" patterns indicative of the formation and orientation of microscopic, anisotropic gel domains. These patterns are related to the creation of *p*H gradients in the sample, enhanced by the production of H^+ and OH^- ions due to electrolysis of H_2O. The presence of a buffer can suppress this behavior, delaying the observation of these light-scattering patterns until production of H^+ and OH^- overwhelms the buffering capacity of the solution. A macroscopic shrinking of the gel away from the cathode, and an increase in the water level at the cathode are noted.

The observed light-scattering patterns are consistent with orientation of rodlike bundles in a direction perpendicular to the *E*-field axis. Results are in qualitative agreement with rodlike models [15,16] that previously have been used to rationalize small angle x-ray and transient birefringence data obtained from agarose gels in the absence of the fields [17,18], as well as being in accord with electron microscopy data [19]. However, although the analysis that we have adopted here to explain the field-induced anisotropic scattering patterns presumes arrays of thin rods, the exact structure of the rodlike domains is unknown and our model should be considered to be but a first approximation. Our microscopy data, for example, suggest a continuum gel structure whose spatial correlations extend over relatively large distances, i.e., of the order of microns. Like our light-scattering data, earlier scattering studies [24,25] also yielded domain sizes of this magnitude. The strong *p*H gradients caused by the H^+ and OH^- ions migrating in opposite directions, and the resulting transport of water toward the cathode, may cause the gel to compress along the direction of the applied field. These effects are likely to be enhanced due to the small amounts of sulfate and other negative charges that are present in HEEO agarose.

Studies of structural changes in gels due to electric fields have relevance in many areas. For example, structural changes linked to transient electric fields interacting with the cytoskeletal matrix lying beneath the plasma membranes of certain cells may be quite significant [26,27]. Similarly, the release of cargo from polymers found within certain secretory vesicles may be modulated by the electric potential across the vesicle membrane [28,29]. Carefully designed *in vitro* measurements that assess the electric-field-induced structural changes of gels like agarose may provide information useful for developing a deeper understanding of such phenomena. Information obtained from these studies also may be useful in designing "smart gels" [30]. Note, too, that the induction of anisotropic gel domains by the electrophoresis of small ions might lead to enhanced separation of large DNA strands.

ACKNOWLEDGMENTS

This research was supported, in part, by the Intramural Research Program of the NIH (NICHD). R.B. acknowledges support from the donors of the Petroleum Research Fund of the American Chemical Society and from NSF DMR.

APPENDIX: CALCULATION OF *p*H

Consider a nonionic gel formed in a solution containing a fully dissolved, simple electrolyte whose positive and negative species are M and χ, respectively. The *p*H profile in the gel can be calculated using one-dimensional diffusion equations to model the migration of the dissolved ions, as done by Hirose *et al.* [7], and then invoking electroneutrality to calculate the local concentration of hydrogen ions. For example, for the positive electrolytic species, one can write

$$\frac{\partial c_M}{\partial t} = D_M \frac{\partial^2 c_M}{\partial x^2} - \upsilon_M \frac{\partial c_M}{\partial x}, \tag{A1}$$

where c_M, D_M, and ν_M denote the concentration, diffusion constant, and electrophoretic velocity of the ion. The diffusion constant and the velocity are proportional to the ion mobility μ_M with $D_M=\mu_M RT/z_M F$ and $\nu_M=\mu_M E$. Using the boundary condition that there are no fluxes of ions at either electrode (i.e., the electrodes are neither a source nor sink for ions), and assuming that the initial concentration of ions is constant along the gel, Hirose *et al.* [7] give the solution of this equation as

$$C_M(x,t) = A_0 e^{2px} + e^{px-rt}\left\{ \sum_{n=1}^{n=\infty} B_n \left[\frac{k_n}{p} \cos(k_n x) + \sin(k_n x) \right] e^{-D_M k_n^2 t} \right\} \tag{A2}$$

where A_0, B_n, k_n, p, and r are given by

$$A_0 = \frac{c_M^0 2pL}{e^{2pL}-1}, \quad B_n = \frac{c_M^0 4k_n [1-(-1)^n e^{-pL}]}{Lp^2\left(1+\frac{k_n^2}{p^2}\right)^2},$$

$$k_n = \frac{n\pi}{L}, \quad p = \frac{\nu_M}{2D_M}, \quad r = \frac{\nu_M^2}{4D_M}. \tag{A3}$$

To calculate the concentration of the negative ions, one need only adjust the values of mobility and charge, and change x to $(L\text{-}x)$ in the equations above. Once the concentrations of positive and negative ions are calculated, the conditions of electroneutrality and dissociation equilibrium of water are used

$$c_{H^+}c_{OH^-} = K_w \quad c_{H^+} + z_M c_M = c_{OH^-} + z_\chi c_\chi, \tag{A4}$$

where c_χ is the concentration of negative ions with charge z_χ, and K_w is the dissociation constant of water, 10^{-14}. Thus $p\mathrm{H}=-\log(c_{H^+})$ can be calculated across the gel sample at different times, given input parameters of mobility and charge of ions, electric field strength, and initial ion concentrations.

[1] D. L. Holmes and N. C. Stellwagen, J. Biomol. Struct. Dyn. **7**, 311 (1989).
[2] J. Stellwagen and N. Stellwagen, Biopolymers **34**, 187 (1994); N. Stellwagen, Colloids Surf., A **209**, 107 (2002).
[3] N. C. Stellwagen, Electrophoresis **13**, 601 (1992).
[4] T. Tanaka, I. Nishio, S. Sun, and S. Ueno-Nishio, Science **218**, 467 (1982).
[5] S. Hirotsu, Jpn. J. Appl. Phys., Suppl. **24**, 396 (1985).
[6] P. E. Grimshaw, J. H. Nussbaum, A. J. Grodzinsky, and M. L. Yarmush, J. Chem. Phys. **93**, 4462 (1990).
[7] Y. Hirose, G. Giannetti, J. Marquardt, and T. Tanaka, J. Phys. Soc. Jpn. **61**, 4085 (1992).
[8] M. Shibayama and T. Tanaka, Adv. Polym. Sci. **109**, 1 (1993).
[9] S. J. Kin, C. K. Lee, and S. I. Kim, J. Appl. Polym. Sci. **92**, 1731 (2004).
[10] E. A. Moschou, S. F. Peteu, L. G. Bachas, and S. Daunert, Chem. Mater. **16**, 2499 (2004).
[11] M. Higa and T. Yamakawa, J. Phys. Chem. B **108**, 16703 (2004).
[12] M. B. Rhodes and R. S. Stein, J. Polym. Sci., Part A-2 **7**, 1539 (1969).
[13] L. Yao and S. Krause, Macromolecules **36**, 2055 (2003).
[14] K. B. Guiseley and D. W. Renn, *Agarose: Purification, Properties, and Biomedical Applications* (Marine Colloids Division, FMC Corporation, Rockland, ME, 1975).
[15] D. A. Rees, Biochem. J. **126**, 257 (1972).
[16] S. Arnott, A. Fulmer, W. E. Scott, I. C. M. Dea, R. Moorhouse, and D. A. Rees, J. Mol. Biol. **90**, 269 (1974).
[17] M. Djabourov, A. H. Clark, D. W. Rowlands, and S. B. Ross-Murphy, Macromolecules **22**, 180 (1989).
[18] Y. Dormoy and S. Candau, Biopolymers **31**, 109 (1991).
[19] S. Whytock and J. Finch, Biopolymers **31**, 1025 (1991).
[20] C. Rochas, A. M. Hecht, F. Horkay, and E. Geissler, Macromol. Symp. **114**, 173 (1997).
[21] T. Shimada, M. Doi, and K. Okano, J. Chem. Phys. **88**, 2815 (1988).
[22] E. Fredericq and C. Houssier, *Electric Dichroism and Electric Birefringence* (Clarendon Press, Oxford, 1973).
[23] S. V. Savenko and M. Dijkstra, Phys. Rev. E **70**, 011705 (2004).
[24] E. Pines and W. Prins, Macromolecules **6**, 888 (1973).
[25] D. Bulone and P. L. San Biagio, Biophys. J. **68**, 1569 (1995).
[26] I. Tasaki and P. M. Byrne, Biochem. Biophys. Res. Commun. **188**, 559 (1992).
[27] I. Tasaki, Jpn. J. Physiol. **49**, 125 (1999).
[28] C. Nanavati and J. M. Fernandez, Science **259**, 963 (1993).
[29] P. E. Marszalek, V. S. Markin, T. Tanaka, H. Kawaguchi, and J. M. Fernandez, Biophys. J. **69**, 1218 (1995).
[30] Y. Osada and S. Ross-Murphy, Sci. Am. **268**, 82 (1993).